Cost-effective Design Options for IsoDAR

A. Adelmann[1], J.R. Alonso[2], W. Barletta[2], R. Barlow[3], L. Bartoszek[4], A. Bungau[3], L. Calabretta[5], A. Calanna[2], D. Campo[2], J.M. Conrad[2], Z. Djurcic[6], Y. Kamyshkov[7], H. Owen[8], M.H. Shaevitz[9], I. Shimizu[10], T. Smidt[2], J. Spitz[2], M. Toups[2], M. Wascko[11], L.A. Winslow[2], J.J. Yang[1,2]

[1] *Paul Scherrer Institut, Villigen, CH-5232, Switzerland*
[2] *Massachusetts Institute of Technology, Cambridge, MA 02139, USA*
[3] *University of Huddersfield, Huddersfield, HD1 3DH, UK*
[4] *Bartoszek Engineering, Aurora, IL 60506, USA*
[5] *Istituto Nazionale di Fisica Nucleare, Laboratori Nazionali del Sud, I-95123, Italy*
[6] *Argonne National Laboratory, Argonne, IL 60439, USA*
[7] *University of Tennessee, Knoxville, TN 37996, USA*
[8] *University of Manchester and Cockcroft Institute, Manchester, M13 9PL, UK*
[9] *Columbia University, New York, NY 10027, USA*
[10] *Tohoku University, Sendai, 980-8578, Japan*
[11] *Imperial College London, London, SW7 2AZ, United Kingdom*

Abstract: This whitepaper reviews design options for the IsoDAR electron antineutrino source. IsoDAR is designed to produce 2.6×10^{22} $\bar{\nu}_e$ per year with an average energy of 6.4 MeV, using isotope decay-at-rest. Aspects which must be balanced for cost-effectiveness include: overall cost; rate and energy distribution of the $\bar{\nu}_e$ flux and backgrounds; low technical risk; compactness; simplicity of underground construction and operation; reliability; value to future neutrino physics programs; and value to industry. We show that the baseline design outlined here is the most cost effective.

Contents

This whitepaper reviews the design options for a decay-at-rest $\bar{\nu}_e$ source [1]. "IsoDAR" is a novel, very high-intensity source that will produce $\bar{\nu}_e$ with $\langle E \rangle = 6.4$ MeV from the beta decay-at-rest of ^{8}Li. When paired with an existing $\sim$1 kton scintillator-based detector, such as KamLAND [2], IsoDAR opens a wide range of possible searches for beyond standard model physics. Refs. [1, 3] discuss the outstanding potential of a search for sterile neutrino oscillations using the L/E dependence of inverse beta decay (IBD) events ($\bar{\nu}_e + p \rightarrow e^+ + n$) within the detector. Beyond this, the source is designed to produce more than an order of magnitude more $\bar{\nu}_e$-electron scattering events than all past $\bar{\nu}_e$ experiments, opening up new opportunities for searches beyond the Standard Model [4, 5, 6]. Studying the production of exotic particles which subsequently decay in the detector is also an interesting goal, as this may relate to the dark matter problem [7].

IsoDAR-like $\bar{\nu}_e$ sources have been considered for underground physics in the past [8, 9, 10]. However, such sources have not led to sufficiently high event rates to reach physics goals. In Ref. [1], we have presented a design which can provide the physics measurements mentioned above. This conceptual design arose while considering an injector for the DAEδALUS (Decay-At-rest Experiment for δ_{CP} studies At a Laboratory for Underground Science) CP-violation experiment [11, 12, 13]. It was recognized that this injector cyclotron could be used as an intense source of $\bar{\nu}_e$. IsoDAR can therefore be considered as part of a phased program to establish the DAEδALUS program.

The base IsoDAR design utilizes a 60 MeV/n high-power compact (as opposed to separated sector) cyclotron. The cyclotron accelerates 5 mA of H_2^+ injected from a conventional ion source at 70 keV. This delivers 10 mA of protons (600 kW, continuous wave) to target as H_2^+ is two protons bound by one electron. The beam impinges on a beryllium target, which produces a very high neutron flux. The neutrons enter a surrounding 99.99% pure ^{7}Li sleeve, thermalize, and capture to produce ^{8}Li. The beta-decay of ^{8}Li produces the $\bar{\nu}_e$ that can be detected in an adjacent scintillator-based detector like KamLAND. We assume a vertex resolution of 12 cm and an energy resolution $6.4\%/\sqrt{E\ (\mathrm{MeV})}$ in the detector, consistent with KamLAND [14]. The most relevant experimental parameters are listed in Table 1.

This base design represents the most cost-effective option for IsoDAR. Here, we present the broad alternatives to this and explain the base design requirements. We begin in Sec. 1 by discussing the criteria for cost-effectiveness, based on the physics goals mentioned above. This is followed by a detailed discussion of our base design in Sec. 2. We explain the partnerships which may significantly add to cost-effectiveness in Sec. 3, many of which are available because of the baseline design choices. We then consider alternatives to the base design. These considerations divide into three areas of study: (1) the fundamental underlying choices of beam particle species, energy, and target material, discussed in Sec. 4; (2) the technology used to deliver the beam to the target, discussed in Sec. 5; and (3) radical alternatives that are dissimilar to the IsoDAR base design, discussed in Sec. 6. In this analysis, we compare to four specific alternatives which appear to be the only other possible options for this source:

1. Radio-frequency quadrupole (RFQ) injection with a separated sector cyclotron.
2. A 30 MeV linear accelerator (LINAC) with a 40 mA proton beam.
3. A β-beam based design.
4. A new detector located at an existing beamline.

In Sec. 7, we conclude that the design outlined in Ref. [1] is the most cost effective approach among the alternatives identified.

Accelerator	60 MeV/amu of H_2^+
Current	10 mA of protons on target
Power	600 kW
Up-time	90%
Run period	5 years (4.5 years live time)
Target	^{9}Be surrounded by ^{7}Li (99.99%)
$\overline{\nu}$ source	^{8}Li β decay ($\langle E_\nu \rangle$=6.4 MeV)
$\overline{\nu}_e$/1000 protons	14.6
Total flux during run	1.29×10^{23} $\overline{\nu}_e$
Detector	KamLAND
Fiducial mass	897 tons
Target face to detector center	16 m
Reconstruction efficiency	92%
Vertex resolution	12 cm/$\sqrt{E\ (\mathrm{MeV})}$
Energy resolution	6.4%/$\sqrt{E\ (\mathrm{MeV})}$
Prompt energy threshold	3 MeV
IBD event total	8.2×10^5
$\overline{\nu}_e$-electron event total	7200

Table 1: The relevant experimental parameters used in this study, reprinted from Ref. [1].

1 Criteria for a Cost Effective Design

We study alternative design options based on the criteria below for cost-effectiveness. In this section, we explain the motivation for these criteria. In the concluding section, we provide parameters for ranking alternative designs. The criteria are:

1. *Cost:* Minimizing the total acquisition and operations costs is important to any project. In the case of running at an existing underground lab, this includes the cost of the accelerator, the target ($\bar{\nu}_e$ source), electricity, and relevant infrastructure that must be provided to successfully conduct the experiment. When we consider running at an existing accelerator, this will include issues of installing a new beamline and detector with sufficient shielding.

2. *Rate and energy distribution of the $\bar{\nu}_e$ flux:* Maximizing the $\bar{\nu}_e$ flux is vital for sensitivity to sterile neutrinos as well as accomplishing the other physics goals. The IsoDAR design produces 2.6×10^{22} $\bar{\nu}_e$ per year with a mean energy of 6.4 MeV. An alternative design must match this or come close. Note that a mean $\bar{\nu}_e$ energy well above 3 MeV is important, as this requirement helps differentiate signal events from (usually less energetic) radiogenic backgrounds in the detector. This is especially important for the $\bar{\nu}_e$-electron scattering and dark matter studies, which rely on single-pulse signals. Note that multiple $\bar{\nu}_e$ sources with endpoints > 3 MeV are acceptable, since the flux is directly measured using the IBD interaction and its well-known cross section [1, 15].

3. *Rate and energy distribution of backgrounds:* The ν_e intrinsic background must be minimized with respect to the $\bar{\nu}_e$ flux, and limited to < 3 MeV. In the case where we study the possibility of running at existing accelerators, we also consider cosmogenic backgrounds under this item. This is relevant at low depth since ^{8}Li has a half-life of 841 ms. A beam spill structure of a

few microsecond or less, as is offered at many existing laboratories, cannot help to distinguish between signal and cosmogenic background.

4. *Low technical risk:* No existing cyclotron can meet our physics goals. Therefore, some R&D is required for the base design. We compare the risk involved to the risk of implementing alternative designs.

5. *Compactness of both accelerator and $\bar{\nu}_e$ source:* Compactness of the accelerator is driven by space considerations underground. The goal is to keep the spatial footprint of the accelerator within a few meters in all dimensions. Compactness of the $\bar{\nu}_e$ source is also important for the sterile neutrino search, in order to make implementation practical. For a $\bar{\nu}_e$ event energy of $\langle E \rangle = 8$ MeV, the sterile neutrino search is optimized for an oscillation length of about 8 m. Thus, the source, including all of its shielding, must be located within about 16 m of the detector in order to successfully reconstruct the oscillation wave.

6. *Simplicity of underground construction and operation:* Along with compactness, application underground encourages the simplest possible design, construction, and operation plans. Cost considerations here also encourage simplicity.

7. *Reliability:* The up-time of the accelerator must comfortably exceed the up-time planned for the experiment so as to ensure successful completion of the physics goals. The experiment only requires 10% downtime in order to measure beam-off backgrounds. Thus, we seek an accelerator which is likely to require low downtime for maintenance.

8. *Value to future physics programs:* Developing engineering and infrastructure for future physics programs is desirable.

9. *Value of this development to industry:* Developing a design which is of interest to industry will lead to strong industrial partnerships and sharing of development costs.

We will touch on each of these points throughout the following text. In the concluding section (Sec. 7), we return to this itemized discussion.

2 The IsoDAR Base Design

The major components of IsoDAR are the ion source, the cyclotron, and the $\bar{\nu}_e$ source. These are connected by beam transport systems, the design of which can be considered straightforward.

2.1 The Ion Source

INFN-Catania has constructed the Versatile Ion Source (VIS) (Fig. 1) [16], which is a non-resonant microwave (2.45 GHz) source capable of very high continuous wave (CW) proton or H_2^+ beams suitable for IsoDAR. Optimization of one or another ion species is obtained by varying gas pressure and microwave power into the source. The performance of the VIS for production of high-quality, high-current H_2^+ ions will be fully characterized at the BEST Cyclotron Systems test stand, where the beam will be injected and accelerated to 1 MeV, producing results valuable to simulations for IsoDAR and the DAEδALUS Superconducting Ring Cyclotron (SRC) beam. However, in comparisons to other technology options, we regard the overall risk concerning the ion source to be low since we have already performed preliminary measurements.

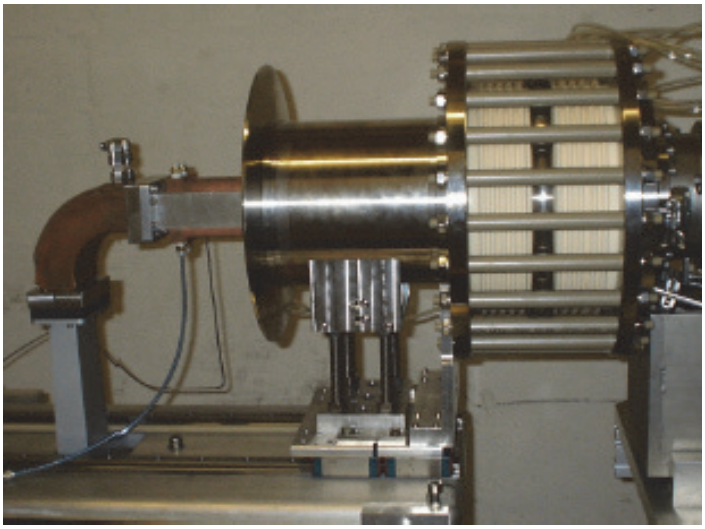

Figure 1: The Versatile Ion Source.

The use of H_2^+ rather than H^- ions or protons is a key step forward in development. H_2^+ is chosen to reduce space charge effects, since it has an electric charge of +1 for every two protons accelerated. Thus, 5 mA of this ion corresponds to 10 mA of protons on target. This is discussed further below.

In our design, a 5 mA H_2^+ beam is injected into the cyclotron at 70 keV (35 keV/amu) via a spiral inflector. For comparison, the generalized perveance (which parametrizes the strength of the space charge effect),

$$K = (qI)/(2\pi\epsilon_0 m\gamma^3\beta^3) \ , \tag{1}$$

is similar to that of existing cyclotrons that inject 2 mA of protons at 30 keV [17]. This gives us confidence that space-charge forces for the IsoDAR 5 mA H_2^+ beam should be manageable. We note, however, that the spiral inflector must be larger than in these lower-energy proton machines.

2.2 The Cyclotron

2.2.1 Introduction to Cyclotrons

It is worthwhile to briefly review cyclotron design and terminology, as we will refer to this information in the text that follows.

A compact cyclotron has a monolithic magnet and circular coil. The alternative to the compact design segments the magnet, leading to a "separated-sector design" such as is used in the Paul Scherrer Institut (PSI) Injector II (3 mA of protons at 72 MeV). Typically, the compact design is most economical at lower energies ($\lesssim$ 100 MeV), but is less flexible than a separated-sector design. The dipole magnet in either case may be resistive, as with IsoDAR, or super-conducting.

In a compact cyclotron, particles from the ion source are injected axially at the center, in our case via a "spiral inflector" which directs the beam from a vertical direction to the horizontal median plane. An RF cavity system accelerates the particles and, as the beam gains energy, the

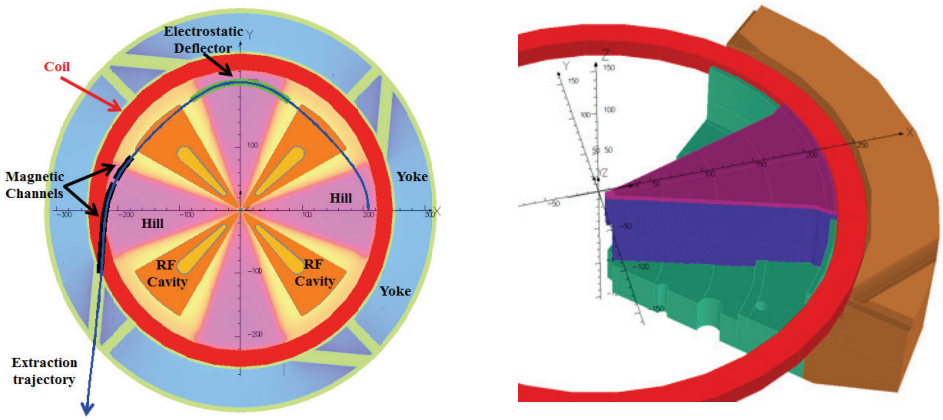

Figure 2: Left: Layout of the cyclotron. Pastel colors represent the magnetic field map (magenta is highest field, yellow is negligible field). Overlaid on the map are the RF cavities (orange) and coil (red). The extraction trajectory for H_2^+ is shown. Right: Illustration of the Opera3D finite element magnetic model showing one quarter of the cyclotron with the pole, the return yoke, and the coil.

trajectory is bent by a dipole magnetic field. As a result, particles follow spiral orbits with radius increasing with energy. The spatial separation between the "turns" grows smaller as the beam approaches the outer edge of the cyclotron.

Achieving more than 10 to 20 MeV/amu requires an "isochronous design" to keep the beam revolution frequency synchronized with the RF field. In an isochronous design, the time for one revolution in the cyclotron is independent of particle energy.

For vertical focusing and to facilitate beam stability, the pole faces are formed into pie-shaped wedges alternating a narrow pole gap ("hill") region with a larger gap ("valley") region. In Fig. 2, the high field regions in magenta correspond to the hills. RF cavities are typically placed in the valley region (yellow in Fig. 2) that has negligible field. The RF cavities are overlaid in Fig. 2 in orange. The IsoDAR cyclotron has 4-fold symmetry in this magnet pole configuration.

2.2.2 Specifics of the Design

The required experimental parameters (see Table 1) are achievable with the IsoDAR base design, shown in Fig. 2 and described in Table 2. This design has been developed as the DAEδALUS Injector Cyclotron (DIC), with technical details provided in Ref. [11].

Fig. 2, left, provides the magnetic field map of the present design, where the hill has 2 T magnetic field and the return yoke (cyan) has -1.5 T. A 3-D rendering of one sector is shown on the right side of the figure. The single circular coil associated with a compact cyclotron is indicated in red on both figures.

Throughout acceleration, the isochronism accuracy, the degree to which the particle revolution frequency matches the RF frequency, in this initial physics model is better than 5.0×10^{-4} and the phase diagram is maintained in a narrow range ($\sim \pm 4°$). Beam quality is not diminished by resonance crossing [18], since this occurs quickly. A second resonance crossing is observed near the extraction region, but accurate beam dynamics simulations have shown that its effect is negligible.

E_{max}	60 MeV/amu	E_{inj}	35 keV/amu
R_{ext}	1.99 m	R_{inj}	55 mm
$< B >$ @ R_{ext}	1.16 T	$< B >$ @ R_{inj}	0.97 T
Sectors	4	Hill width	28 - 40 deg
Valley gap	1800 mm	Pole gap	100 mm
Outer Diameter	6.2 m	Full height	2.7 m
Cavities	4	Cavity type	$\lambda/2$, double gap
Harmonic	6th	RF frequency	49.2 MHz
Acc. Voltage	70 - 240 kV	Power/cavity	310 kW
ΔE/turn	1.3 MeV	Turns	95
ΔR /turn @ R_{ext}	> 14 mm	ΔR/turn @ R_{inj}	> 56 mm
Coil size	200x250 mm^2	Current density	3.1 A/mm^2
Iron weight	450 tons	Vacuum	$< 10^{-7}$ mbar

Table 2: Parameters of the DAEδALUS injector cyclotron, from Ref. [11].

Other features of the design, including RF frequency, harmonic number, and the average field value (see Table 2), are selected to match the DAEδALUS SRC. This potential future use of the IsoDAR cyclotron adds to the cost-effectiveness and does not diminish the design in any way. The large hill gap of 10 cm allows ample space for the beam envelope, and provides good conductance for the $< 10^{-7}$ mbar vacuum required to minimize beam loss due to interactions with residual gas. Vacuum pumping will be provided by eight cryopanels located in the valley regions, possibly integrated with the RF cavities. The angular width of the hill, in the range 28° to 40°, allows for adjustments to optimize isochronism and vertical focusing. All of these parameters will be studied to provide an optimal design.

2.2.3 Results of Simulation

Within the DAEδALUS design effort, extensive and precise simulations targeting the most challenging aspects of high power hadron drivers have been pursued. These studies, mainly of stationary distributions and losses, are reported in Refs. [11, 19].

The beam dynamics model is based on the OPAL (Object Oriented Parallel Accelerator Library) software framework [20]. The model is validated using measured data from the PSI high power Ring Cyclotron (1.4 MW $\approx$ 590 MeV $\times$ 2.4 mA continuous wave) [21].

The main conclusions from the study relevant for IsoDAR (from Ref. [19]) are:

1. The simulation shows that beam transport in the cyclotron is space-charge-dominated. Interestingly enough, however, these space-charge forces are high enough to yield longitudinal stability of the bunch.

2. No flattop cavity is (therefore) required and the four valleys are available for installing the accelerating cavities.

3. For an extraction energy of 60 MeV/amu, the cyclotron needs 106 turns (comparable with the 72 MeV Injector II at PSI).

4. The H_2^+ beam can be extracted with beam loss on septum of less than 150 W for 100% duty cycle, which will not result in significant issues at extraction (the last turn separation is 20 mm; for comparison the PSI Injector II has 20.5 mm).

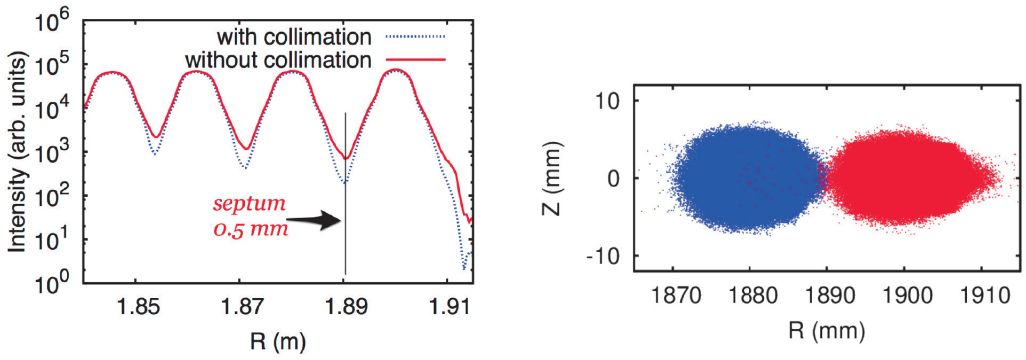

Figure 3: Object Oriented Parallel Accelerator Library simulations for 5 mA of H_2^+ beam in the DAEδALUS Injector Cyclotron. With proper beam forming collimation in the central region, less than 1% of the beam will be intercepted by a 0.5 mm septum demarking the extraction channel. The figure on the right shows the next-to-last (blue) and last turn (red) as it enters the extraction channel. The overlap of the final turn with the preceding one is small as the beam halo is minimal. The figure is from Ref. [19].

2.2.4 Extraction

IsoDAR's baseline plan for extraction is to use an electrostatic septum. As described in the previous section, the last turn separation of 20 mm allows for such a system to extract the beam with low losses. Figure 3 shows the results of beam simulations, demonstrating that less than 1% of the beam is lost on a 0.5 mm septum.

Furthermore, as H_2^+ ions are employed, a narrow and thin stripper foil can be placed upstream of the septum which will intercept all particles that would hit the septum. The resulting two protons from the ion will spiral inwards and avoid the septum altogether. These can be collected with a suitably-placed catcher which may be made to take substantially more heat than the septum.

Thus, the electrostatic-septum extraction system is seen as low risk and allows for synergy with future physics projects, such as injection for the larger DAEδALUS SRC and with the medical industry, as we discuss below. This can therefore be considered a practical and cost-effective solution.

Foil-stripper extraction may seem advantageous over electrostatic extraction because of the preponderance of stripping in modern commercial cyclotrons in this energy range. These machines, such as the Cyclone 30 IBA [22] and TR-30 EBCO [23], accelerate 30 MeV H^- beams which, after stripping, are bent in the opposite direction to easily leave the cyclotron. The two protons (after stripping the H_2^+) will spiral inwards and, because of the hill/valley field variations, an extraction channel could be designed to bring the beam out. However, care is needed in order to avoid the central region with the axial injection components. Foil lifetime in IsoDAR's very high currents would be a serious consideration. The mean life of the IBA and EBCO stripper foils is 20-40 mA·h. That is, the foil lasts 20-40 h [24] with a beam current of 1 mA. The 70 MeV Legnaro cyclotron proposes to use a 6-stripper carousel to achieve a continuous operation of 14 days, with a maximum beam current of 0.7 mA. However, foil lifetime is substantially shortened at higher beam currents, and with a single stripper station it is unlikely that a foil could be found that would have a practical lifetime when exposed to a 5 mA beam.

2.2.5 Assembly Underground

Transport and assembly of an accelerator underground presents engineering challenges. In the case of IsoDAR, the cyclotron weighs around 500 tons and is approximately 5 m in diameter when fully assembled. Larger or more massive designs are likely to be unfeasible. Access drifts to the underground space presents an important constraint. Using KamLAND tunnels as an example, the narrowest size is 2.7 m in width and 3.2 m in height [25]. The minimum diagonal length is therefore 4.2 m. This constraint requires a design that can be broken down into smaller pieces.

The IsoDAR base design meets this requirement. The iron pieces are readily accommodated. The yoke and return slabs do not have dimensional criticality, so can be bolted or welded once transported to the cavern. Pole pieces are a little more challenging as each of the hills must be machined as a discrete part in order to minimize field inhomogeneities from dimensional variations. The welds must be made in the valleys where the field is negligible. In our design, each hill is a wedge of radius approximately 2 m, arc length of approximately 1.5 m, and thickness less than 1 m. These should present no transport problems. The pole base, to which the hill sections are bolted, will have an assembled diameter of 4 m. To reduce total weight, the base can be built up from several disks of 15-30 cm thickness, which will be brought into the hall tilted diagonally. Most other components of the cyclotron are not an issue. Each of the RF cavities will fit into the valley sections of the poles and transport is therefore is not a problem. The vacuum chamber must encompass the entire inner region of the cyclotron, but can be made from sections welded together or using pole pieces themselves for vacuum surfaces.

The primary underground assembly issue is the coils. The inside radius of each of the two coil packages is 4.1 m and the cross section of each coil package is 20×25 cm, so that the outer diameter is 4.5 m. This means that an intact coil cannot be brought underground, even when tilted on the diagonal. Two alternative solutions for assembling the coils are now under study. First, it is possible to wind in place, but this would require transport and assembly of substantial tooling equipment, and so appears to be least cost-effective. The favored alternative is segmenting the coil. To understand this technique, we an look to the TRIUMF cyclotron, which has a coil constructed from six segments. The TRIUMF conductor is made from aluminum plates approximately 2 cm thick and 60 cm high, with 18 such plates bundled together to make a segment of the coil. At the ends of each of the six segments, each plate is welded to its corresponding plate in the adjacent section. The result is a single monolithic coil which, in the case of TRIUMF, is 18 m in diameter. Our case is significantly less challenging. Dividing the coil into two segments would be sufficient for transport into the cavern, so only two weld sections would be needed. Power supplies that provide 15 kA allow only 10 turns for the necessary 150 kA. Welding 10 turns is feasible, low risk, and would be cost effective.

Care must be taken in planning the staging, assembly and rigging of the device underground. The heaviest pieces are expected to be less than 50 tons. Several options can be explored to minimize assembly issues, and possibly ease the requirements for cranes. One would be the building of a jacking structure capable of lifting the entire upper pole and yoke assembly, and then possibly sliding it in place over the lower yoke/pole. This structure, similar to one installed at TRIUMF, would also provide a way of efficiently splitting the magnet steel for access to the mid-plane. This access is extremely important, and must be provided. Another option would be to mount the entire cyclotron in the vertical plane. The pole pieces could then be mounted on substantial rails, and splitting accomplished by sliding the magnet halves apart along the rails. The geometry of the return yoke is fairly arbitrary, and does not need to be circular. A square configuration could provide adequate steel for containing the flux, and would facilitate mounting and support of the

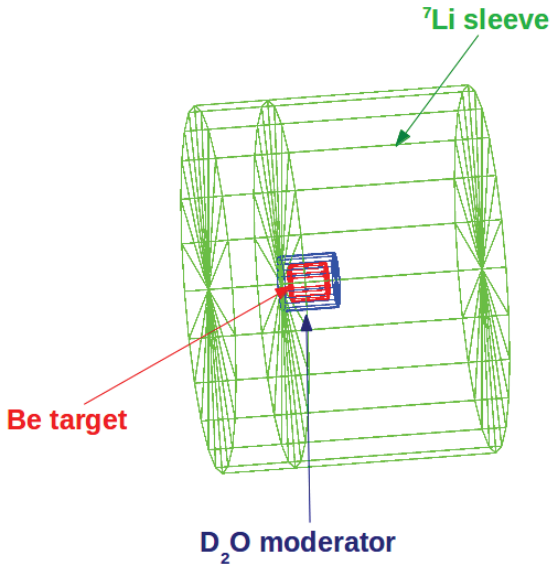

Figure 4: The beryllium target surrounded by the ^{7}Li sleeve. The sleeve is 150 cm long and has a 200 cm outer diameter.

cyclotron in a vertical orientation. A vertical orientation for the cyclotron plane also eases another problem: the axial injection line will require about 4 m of space between the ion source and the spiral inflector at the cyclotron mid-plane. If the cyclotron plane is horizontal, this axial injection line must be vertical, or must have a 90° bend, complicating the optics and transport of the intense beams from the ion source. With a vertical cyclotron plane, the axial injection line is horizontal, and can be accommodated with much greater ease.

In all, while presenting some interesting engineering challenges, the transport and installation of the IsoDAR cyclotron underground is feasible.

2.2.6 Duty Factor, Beam Structure Requirements and Total Availability

The half-life of ^{8}Li is 841 ms. Therefore, the experiment does not benefit from having a machine with a narrow pulse time structure. With regard to time structure, the IsoDAR cyclotron can be considered a CW source and is therefore a good match to the requirements.

We assume 90% beam availability to reach the physics goals. This is set by the need for beam-off data in order to measure backgrounds. Since there are no beam-structure requirements, the 10% downtime can be scheduled as needed to accommodate maintenance. PSI recently achieved a week with 99.95% up-time [26] and the TR30 cyclotron (30 MeV, 1.2 mA) averages 98.3% uptime [27].

2.3 The Beam Transport Line

The 10 mA of 60 MeV/amu beam will be transported from the cyclotron to a target system designed to maximize the $\bar{\nu}_e$ flux from isotopes that decay-at-rest with high Q-value. In consideration of target cooling and degradation and given the 600 kW beam power, we require a uniform beam distributed across the 20 cm diameter target. This can be easily accomplished with wobbler magnets: two orthogonal dipoles excited sinusoidally (and 90° out of phase) that sweep the beam in a circular pattern. Adequate uniformity and sharp falloff can be obtained using several concentric

circular sweeps, from varying the sinusoidal driving voltage. Such a system can achieve ±2% uniformity over a 30 cm diameter field [28], which is substantially larger than is required for IsoDAR. Spreading the beam in this fashion reduces the power density on the target to about 2 kW/cm^2. As this is a CW source rather than a pulsed beam, there are no risks of shock heating or thermal ratcheting.

2.4 The Antineutrino Source

The $\bar{\nu}_e$ source consists of a beryllium target surrounded by a 99.99% isotopically pure ^{7}Li sleeve. There is a 5 cm layer of heavy water moderator in between the target and sleeve. This geometry is shown in Fig. 4. We provide details of the base target and sleeve designs in the following section.

2.4.1 The Target

The main purpose of the target is to produce a large number of neutrons through the interaction of the beam with beryllium. Beryllium has a high neutron production rate because the neutron binding energy is only 1.66 MeV. Although the protons range out in < 3 cm, a target length optimization study finds that secondary neutron interactions contribute significantly to the total ^{8}Li (and resulting $\bar{\nu}_e$) rate. We have optimized the length of the beryllium target to 20 cm, leading to a 10% $\bar{\nu}_e$ flux contribution from the target alone.

The energy deposition (dE/dx) in the target varies as roughly $1/E$, with the Bragg peak at $\sim$ 2 cm. This places the highest heat deposition at the end of the proton range, where proton energy is low and neutron production is small. Pure beryllium is therefore not required here. In response to this, we are considering a segmented target, with a disk of BeO at the region of the Bragg peak. A ceramic that is easily available commercially, BeO has a high thermal conductivity (330 W/m·K) and melting point 2507°C. We note, however, that BeO cannot be used for the entire target because the oxygen substantially diminishes neutron production.

An alternative is to design for a beryllium target that can handle the IsoDAR power deposition of 2 kW/cm^2. A beryllium target for boron neutron capture therapy was demonstrated [29] at MIT-LABA that could withstand 6 kW/cm^2, using a water-based cooling system at the back of the disk. While this design has been deemed feasible, we consider it riskier than the design with the BeO insert at the Bragg peak region.

D_2O is used for target cooling because interactions of fast neutrons from the target inside of this volume increase the total neutron flux. This also provides moderation of the fast neutrons before they enter the sleeve.

Beryllium and BeO are light targets and therefore produce mostly short-lived isotopes upon activation. Using low-A materials reduces the risk related to removal and storage of the activated target. We discuss this further when considering alternative target materials below. The radioactive target handling design will be based on the successful MiniBooNE horn and target handling system. As already stated, the volume that receives the primary physical stress and dose is small and the coffin system can therefore be expected to be much more compact than MiniBooNE's.

The target and sleeve must be engineered for the highest possible reliability. The goal is for the target to last for the full length of the experiment and not have to be changed during the run. Infrastructure for handling the highly radioactive target would be very difficult to integrate into the confined area allocated for it, and changing a target would inevitably require a substantial down-time for the experiment.

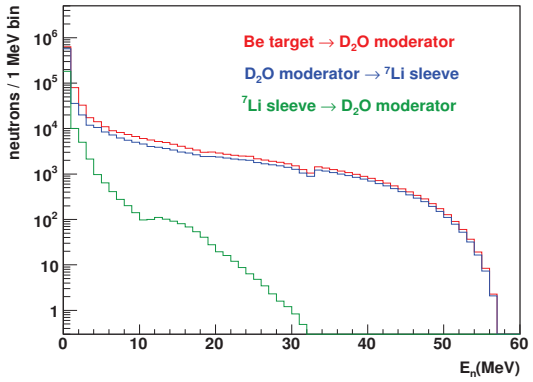

(a) Energy spectra of neutrons exiting the target and entering the heavy water moderator (red), exiting the moderator and entering the sleeve (blue), and of neutrons reflected back into the moderator from the sleeve (green).

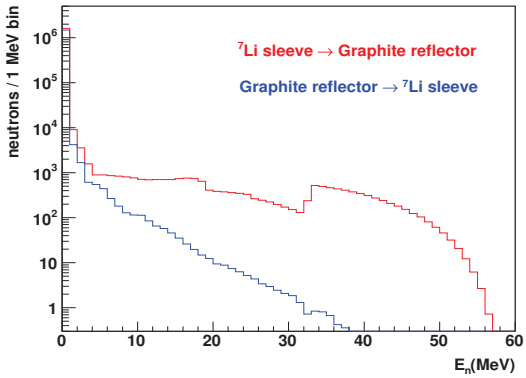

(b) Energy spectra of neutrons exiting the sleeve and entering the reflector (red) and neutrons reflected back into the sleeve (blue).

Figure 5: Energy spectra of neutrons as they pass the most relevant geometric boundaries from one volume to another.

2.4.2 The Sleeve

A sleeve surrounding the neutron source target produces the majority of the $\bar{\nu}_e$ flux. The 150 cm long, 200 cm outer diameter cylindrical sleeve surrounds the target and D_2O layer. This volume is embedded 40 cm into the upstream end of the sleeve; a window allows the beam to impinge on the target. The sleeve, composed of 99.99% isotopically pure ^{7}Li, utilizes thermal neutron capture and the subsequent beta-decay of the resulting ^{8}Li for $\bar{\nu}_e$ production. A neutron reflector, composed of graphite and steel, surrounds this volume. The geometry of the sleeve and the position of the target inside have been chosen to maximize $\bar{\nu}_e$ production in consideration of, among other things, the KamLAND tunnel space restrictions.

The energy spectra of neutrons exiting the target as well as exiting the sleeve can be seen in Fig. 5. Reflected neutrons at both geometric thresholds can also be seen in the figure. Neutrons which thermalize and subsequently capture produce ^{8}Li. Fig. 6 shows the isotopes produced for 10^7 protons on target at 60 MeV. The isotope production rates shown set the benchmark for comparisons of alternative target and sleeve materials below.

Isotope production rates are based on software simulation studies with GEANT4 [30]. GEANT4 provides a large set of hadronic models (data-based, parameterized, and theory-driven), each model being defined for a given type of interaction within a specific energy range. For this particular application, the "QGSP-BIC-HP" physics package was chosen. The most relevant physics model for our study is the pre-compound nuclear implementation utilized by the Binary Cascade (BIC) model. The following hadronic processes are included: inelastic scattering, elastic scattering, neutron fission, neutron capture, lepton-nuclear interactions, capture-at-rest, and charge exchange. Neutrons with energy below 20 MeV are treated with the high-precision (HP) model and the ENDF/B-VII [31] data library. The low-energy GEANT4 software has been well-benchmarked due to use in medical physics [32].

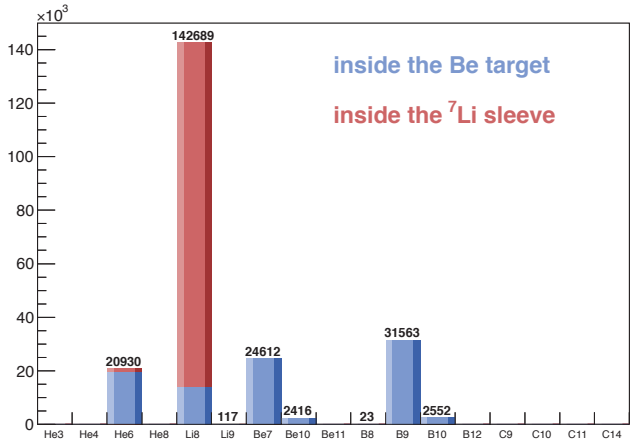

Figure 6: Isotopes produced inside the target and sleeve geometry for 10^7 protons on target, given the baseline IsoDAR design and 99.99% ^{7}Li target sleeve purity.

		<25 MeV		>25 MeV	
Material	density (g/cm^3)	g/cm^2	cm	g/cm^2	cm
Iron	7.8	100	12.8	138	17.7
Concrete	2.4	40	18.8	65	27.1

Table 3: Attenuation lengths for neutrons in iron and concrete.

2.4.3 Shielding

The target, sleeve, and graphite reflector are embedded in a steel and concrete shield. We assume 3.5 m of shielding here. Table 3 provides the attenuation lengths of concrete and iron at neutron energies of <25 MeV and >25 MeV. This volume meets the required rates for occupancy and also provides sufficient shielding to address issues of activation in the mine. The shielding is also adequate for eliminating neutrons that can mimic an antineutrino signal in the detector itself. Those isotopes that are produced in the shielding represent a negligible contribution to the IsoDAR source above ∼3 MeV. As can be seen in Fig. 5, the majority of neutrons that exit the sleeve are "fast" as the volume is well-designed to absorb thermal neutrons.

The compact shielding volume is important within the context of the experiment. If IsoDAR is run at KamLAND, then the source would be placed in a space that presently houses a control room. This room would be relocated, allowing the necessary proximity, including shielding, to the KamLAND detector.

2.5 Flux and Event Distributions

Fig. 7 shows the flux and event rates from the $\bar{\nu}_e$ source expected in KamLAND (897 ton fiducial volume), with detector center located 16 m from the target face. In 5 years, nearly one million IBD events and 7200 $\bar{\nu}_e$-electron scatters will be detected. The physics allowed by this event sample is discussed in Ref. [1]. Any alternative design must meet these rates in a cost-effective manner.

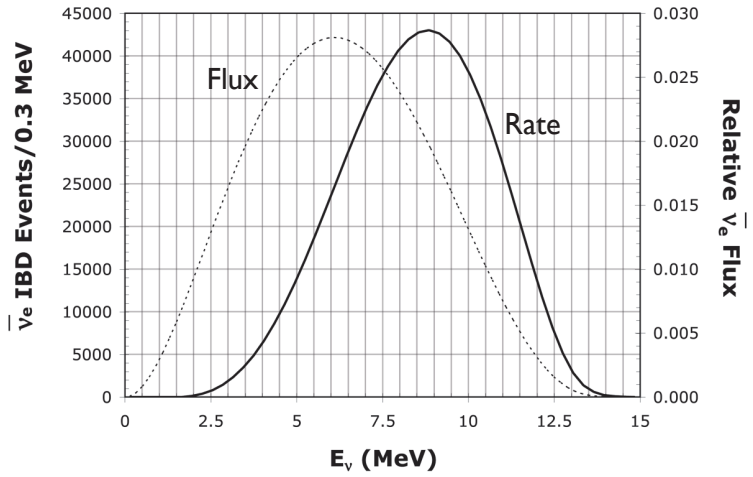

Figure 7: The flux and IBD event distribution expected with the baseline IsoDAR design.

3 Partnerships Allowed By The IsoDAR Base Design

The design of the IsoDAR accelerator has been influenced by potential partnerships with industry and with other particle physics experiments. This is essential to the cost-effectiveness of the experiment. Thus, when weighing the design choices, we have kept in mind the impact of design changes on partnerships. Here, we consider the potential needs of these partnerships.

3.1 With the Medical Isotope Industry

IsoDAR opens the opportunity for a partnership between neutrino physics and industry, an aspect that adds considerably to the cost-effectiveness of the base design. Cyclotrons are widely used to produce medical isotopes. A 60 to 70 MeV machine produces a unique set of isotopes not available at lower energies, summarized in Table 4. The latest generation of accelerators at 70 MeV, running at 750 μA, are sold by IBA [33] and BEST [34]. IsoDAR's 10 mA of protons will lead to a substantial increase in production of these isotopes. Ref. [35] provides a tutorial on isotope production and its connection to IsoDAR.

Isotope	Half-life	Use
^{52}Fe	8.3 h	The parent of the PET isotope ^{52}Mn and iron tracer for red-blood-cell formation and brain uptake studies.
^{122}Xe	20.1 h	The parent of PET isotope ^{122}I used to study brain blood-flow.
^{28}Mg	21 h	A tracer that can be used for bone studies, analogous to calcium.
^{128}Ba	2.43 d	The parent of positron emitter ^{128}Cs. As a potassium analog, this is used for heart and blood-flow imaging.
^{97}Ru	2.79 d	A γ-emitter used for spinal fluid and liver studies.
^{117m}Sn	13.6 d	A γ-emitter potentially useful for bone studies.
^{82}Sr	25.4 d	The parent of positron emitter ^{82}Rb, a potassium analogue. This isotope is also directly used as a PET isotope for heart imaging.

Table 4: Medical isotopes relevant at IsoDAR energies, from Ref. [36].

Several national research laboratories – e.g. ORNL and BNL in the US, INFN-Legnaro in Italy, and ARRONAX in Nantes, France – are seeking to acquire, or are actually using high-power cyclotrons in IsoDAR's energy range for isotope production. ARRONAX has installed the first IBA C70 (0.75 mA, 70 MeV proton cyclotron) [37] and ORNL is requesting funds for a similar machine [38]. Furthermore, BNL conducted a DOE-funded study with Jupiter [36] for a machine in this energy range and Legnaro is acquiring a 70 MeV, 1 mA cyclotron from Best Cyclotron Systems [39].

The programs to be pursued at all of these laboratories involve research with isotopes, ultimately for medical or industrial applications. Legnaro intends, in addition, to collect and accelerate selected ions in a RIB (Radioactive Ion Beam) facility. Target development is a primary goal in their research programs. The delicate process of extracting desired isotopes places unique demands on targets, with a limiting factor always being the power that can be absorbed. Research to increase the power-handling capabilities of targets–enabled by the higher beam currents from IsoDAR-class machines– will ultimately lead to increased yield and improved efficiency in isotope production.

In addition, the high currents can be used for exploring methods for sharing beam between many target stations. This would provide for an overall increase in product output, or versatility in simultaneous production of various isotopes at different target stations.

An elegant solution for such beam sharing is proposed for an H_2^+ beam extracted with a conventional electrostatic septum. The transport line from the extraction point includes a set of focusing elements that form the beam into a long horizontal shape. A stripping foil intercepts a small amount of the beam at one of the lateral edges, the amount intercepted depending on how far in the stripper is moved. Downstream of the foil will be protons for the ions going through the foil, and H_2^+ ions that have missed the foil. This beam is passed through a dipole magnet that bends the protons more strongly into a separate channel where they are focused and transported to a target.

The remaining H_2^+ ions are passed through another focusing element that again produces an elongated beam at the site of a second stripper, with a dipole behind it to again separate protons to be directed to the second target. This process can be repeated as often as desired, for 1 mA per target in principle as many as ten times.

3.2 In Particle Physics

As has been shown for the IsoDAR experiment, 60 MeV proton beams can be prolific sources of neutrinos through the production of beta-decaying isotopes. While IsoDAR is the first of this class of experiments, undoubtedly others will be proposed in the future. Accelerators for such new experiments can build on the base of experience gained with IsoDAR to provide performance tailored to their needs.

Perhaps more relevant, the IsoDAR cyclotron can also be used in a chained-cyclotron system for applications in particle physics. IsoDAR was originally conceived as an injector for the DAEδALUS system, which uses "accelerator modules" with sub-units consisting of an ion source, an injector cyclotron that accelerates to 60 MeV/amu, a SRC that accelerates to 800 MeV, and a target/dump for pion production [12]. In a chained cyclotron system, there is value in accelerating H_2^+ in the injector, and extracting the ion electrostatically. This means that the intact H_2^+ can be extracted at high energy using multiple foils and provides a very clean extraction mechanism at 800 MeV. In principle, H^- can also be extracted by stripping foils, but is not considered a candidate because Lorentz dissociation sets in well before 800 MeV.

3.3 ADS Technology

High power accelerators are of interest to the nuclear reactor community for the purpose of accelerator driven systems (ADS) for thorium reactors and actinide incineration. The interest in thorium reactors has risen worldwide since the Fukushima accident in Japan. These reactors are inherently safe because they produce fission without achieving criticality, so that when the driver shuts down, the reactor turns off. ADS requires very high power and very high reliability. Thus, an attractive system which could be cost effective is to use multiple few-MW cyclotron systems as drivers. Cyclotrons are inherently highly reliable and, with multiple systems, one can be brought down for maintenance while the others continue to drive the reactor. Cyclotrons are sufficiently low-cost that several can be employed per reactor. In fact, the DAEδALUS design originated from a cyclotron for ADS development [40]. Note that there continues to be substantial interest in a chained cyclotron system for this application [41].

4 Alternative Options for the Beam and Antineutrino Target

Having defined the base design and explained the important partnership opportunities it affords, we can now begin to consider alternatives. In this section we begin by considering variations on the basic concept of 60 MeV H_2^+ impinging on a beryllium target surrounded by 99.99% pure ^{7}Li. We consider various beam particles, target materials, and sleeve materials.

4.1 H_2^+ versus other Beam Particles

The viable alternatives to H_2^+ are high energy deuterons, protons, and H^-. The argument against deuterons lies in activation issues. The main arguments against protons and H^- and are in added cost due to –as we will see– the requirement for larger machines in order to mitigate space-charge effects. Opportunities for partnerships discussed above also disfavor protons and H^- compared to the choice of H_2^+.

First, let us consider a beam of deuterons. Each accelerated deuteron ion would deliver one 60 MeV proton and one 60 MeV neutron to the target. Delivering neutrons directly to the target, rather than relying on secondary production, seems naively attractive. However, the problem is in slowing the neutrons so that they productively capture to make ^{8}Li, rather than escaping and activating the surroundings. We find that 60 MeV neutrons are very difficult to control and use successfully. The scattering length of neutrons in beryllium or solid lithium at 60 MeV is more than 20 cm. In other words, the attenuation length is large on the scale of the target/sleeve configuration. As a result, it is difficult to envision a realistic target geometry for a deuteron beam which produces rates at the level of the standard IsoDAR design. We have explored various deuteron beam energies and have not found an optimal design that produces the required rates. Beyond problems with the neutrino source, high energy deuterons are infamous for producing losses in accelerators that are difficult to control. Thus, we reject a deuteron beam because there is no good technical solution for producing a high antineutrino flux while maintaining low activation.

As an example of a comparable proton-based cyclotron, consider the PSI Injector II. This device has a diameter twice the size of IsoDAR's base design and has extracted protons of 72 MeV at 3 mA. Can this technology be extended to 10 mA of protons? Based on simulations with a compact cyclotron design, one expects a significant increase of losses between 5 and 10 mA when running protons. We expect similar effects in a separated sector machine, like PSI II, although the detailed simulation is not complete. The increase in losses is due to space charge effects and can be mitigated by making the machine even larger. However, the PSI-II design, at twice the physical

size of IsoDAR's base design, would be extremely difficult to implement underground. Another problem with proton-based machines is that the staggered foil system described in Sec. 3.1 cannot be applied for protons, and it is unclear how high power isotope production would operate in this case.

An H^- machine also presents difficulties. Similar space-charge issues are applicable for H^- at high intensity, since the charge-per-proton ratio is the same as for a proton in absolute value. Therefore, a PSI-II size design would be the minimum required. Several other problems arise because the H^- is an ion. First, the vacuum must be substantially better than required for a proton machine, and at least comparable to that of the H_2^+ machine, because of stripping with residual gas. Second, the H^- maximum magnetic field must be lower than 1.7 T, to avoid electromagnetic disassociation, making the H^- machine even larger than the proton PSI Injector II cyclotron, which has a hill field of 2 T.

Extraction from an H^- cyclotron can be accomplished either by the same electrostatic septum system that would be employed for a proton machine such as the PSI Injector II, or by using stripping foils. Septum extraction would preserve the H^- ion, which could be distributed to many target stations by the staggered-foil distribution system described above. However, the usual extraction system for H^- cyclotrons used in the isotope industry employs stripping foils at the outer radius of the cyclotron. H^- ions traversing these foils lose both their electrons and are bent out of the cyclotron magnetic field towards an extraction channel. Several (three or four, depending on the symmetry of the cyclotron magnet) strippers can be placed at the outer radius, and beam shared amongst them, to distribute the total beam power to different targets. Sharing the beam on several strippers also mitigates the problem of heating in the foil, which severely affects foil lifetimes. During operation, the foils glow white-hot, perilously close to the sublimation temperature of the carbon foil material. Industry experience is that at around 1 mA a foil will last about 40 hours, an acceptable lifetime given suitable carousels to exchange foils quickly. Higher current through a foil will decrease lifetime in a highly non-linear fashion; a factor of two will cause almost instantaneous failure.

Stripping extraction from a 10 mA H^- cyclotron suitable for the IsoDAR experiment presents an insurmountable problem. This is particularly true since only one extraction channel can be used to bring all of the beam onto the antineutrino-producing target. Thus, an H^- machine would have to be septum-extracted and, as indicated above, would be at least on the order of the PSI Injector II.

Furthermore, for the application of medical isotope production using staggered foils, there is an issue of foil lifetime. When stripped, electrons circle back and are intercepted by the foil. H^- has a larger electron-to-proton ratio than H_2^+ and therefore a reduced foil lifetime. The sum of these problems means that H_2^+ is preferable.

Lastly, an H_2^+ machine is required if the machine is to be employed as an injector in a chained cyclotron system that accelerates beam beyond about 590 MeV. This is the energy where H^- becomes impractical due to the problem of Lorentz stripping. This energy is too low for ADS in thorium reactors [41] or for future neutrino experiments like DAEδALUS. H_2^+ is therefore required for partnerships like these.

4.2 Beam Energy Versus Current

The basic concept behind IsoDAR physics is to flood a volume with neutrons for creating beta-decaying isotopes and the resulting antineutrinos. This is done with 5 mA of H_2^+ (equivalent to 10 mA of protons) at 60 MeV/amu in the base design. However, accelerated particle beams with

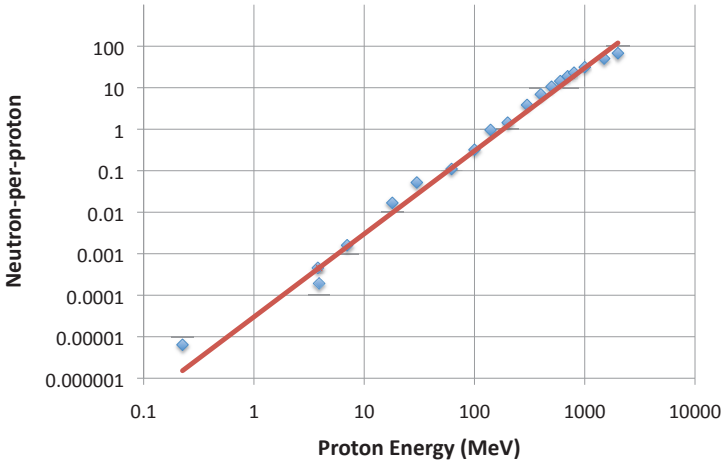

Figure 8: Neutron yield per accelerated particle (proton or deuteron) versus beam energy. The data are fron Refs. [44, 45, 46].

a wide range of energies on various target materials can also provide a high flux of neutrons. One can look at options from about 200 keV to >GeV, from low energy D-T generators [42] to 3 GeV spallation sources [43] – the options available throughout the field are enormous. It is reasonable to ask if any of these systems could provide a viable alternative combination of energy and current to meet IsoDAR's physics goals.

The critical parameter is the n/p ratio, or the number of neutrons produced for every incoming proton striking the target. This ratio is highly dependent on the beam energy. Jongen [44] has compiled n/p data for low energy beams, from D-T generators at less than 1 MeV to about 140 MeV. For higher energies, the ratio is addressed in spallation source studies. It is found that, for energies of 1 GeV and above, the ratio becomes constant for a given beam power. For example, a 2 GeV beam will require half the protons of a 1 GeV beam to generate the same number of neutrons. A graph of neutron production versus beam power is presented by Pynn [45] that covers energies from about 100 MeV to several GeV. A detailed experimental study at 62 MeV [46] provides a specific measurement of this ratio near IsoDAR's energy.

Figure 8 summarizes these data sets, with the red line being an empirical fit to the data points. The data sets match well at the overlap point, including the measurement at 62 MeV, most relevant for IsoDAR. The straight line (on a log-log scale) corresponds to a quadratic relationship in n/p versus beam energy over almost 4 orders of magnitude for beam energy, with

$$(n/p) = 3 \times 10^{-5} \times E^2 \ , \tag{2}$$

where the energy E is in MeV.

Table 5 displays the n/p ratio as a function of energy, and assesses the beam currents necessary for IsoDAR's antineutrino production: 2.6×10^{22} $\bar{\nu}_e$ per year with 10 mA of protons at 60 MeV.

We have chosen 60 MeV as the ideal beam energy given the constraints of underground application and cost. It is clear that below 60 MeV the performance of existing accelerators falls far short

Beam energy MeV	n/p	n/p (fit)	Req'd current	Max. Existing	Source
0.225	6.40E-06	1.51875E-06	710 A	10 mA	D-T gen.
3.9	1.92E-04	4.56E-04	2.4 A	2 mA	IBA
3.8	4.56E-04	4.33E-04	2.5 A	2 mA	IBA
7	1.60E-03	1.47E-03	730 mA	2 mA	IBA
18	1.68E-02	9.72E-03	110 mA	2 mA	IBA
30	0.052	0.027	40 mA	0.8 mA	IBA
60		0.11	10 mA	10 mA	IsoDAR
62	0.11	0.12	9.4 mA		
100	0.32	0.3	3.6 mA		
140	0.96	0.588	1.8 mA	1 mA	IBA
200	1.44	1.2	900 μA		
300	3.84	2.7	400 μA		
400	6.912	4.8	230 μA		
500	10.56	7.5	140 μA	0.2 mA	TRIUMF [47]
600	14.4	10.8	100 μA	2.2 mA	PSI [48]
700	18.816	14.7	70 μA		
800	23.04	19.2	60 μA	1 mA	LANSCE [49]
1000	31.2	30	40 μA	1 mA	SNS [50]
1500	50.4	67.5	20 μA		
2000	67.84	120	10 μA		

Table 5: Data for n/p ratio versus energy, from Refs. [44, 45, 46]. The "n/p (fit)" column presents values from a linear regression fit to a quadratic relationship between n/p and energy. The "Req'd current" column lists the current needed at each energy to generate the flux of $\bar{\nu}_e$ required for the IsoDAR experiment.

of meeting the required antineutrino flux goals. While the higher energy (>500 MeV) machines easily meet this requirement, they will be considerably larger and more expensive. This precludes serious consideration of higher energies for IsoDAR.

4.3 Alternative Target and Sleeve Materials

Having determined that a 60 MeV/amu H_2^+ beam on target is optimal, we can now explore alternative target and sleeve materials. We begin by considering the baseline target composed of ^{9}Be and compare the neutron output to heavier targets. Then, we consider materials that can be used in the sleeve for optimizing $\bar{\nu}_e$ production.

4.3.1 Alternative Solid Target Materials

The choice of target material is guided by engineering and cost requirements. At the low-A end of the periodic table, it must be noted that several isotopes with $Q > 3$ MeV can be produced at relatively high rates which decay to neutrinos, rather than antineutrinos, including ^{8}B and ^{12}N. The suppression of these isotopes is important in the choice of materials considered here. This eliminates carbon and some other potential low-A target materials. At the high-A end, we avoid already-activated materials, such as depleted uranium, for ease of use.

The total ^{8}Li yield calculated for various incident proton energies and with copper and tungsten targets for comparison with beryllium is presented below. The alternative target materials are considered because they meet the following guidelines:

- High neutron yield.
- High melting point.
- High thermal conductivity.
- Chemically inert, low corrosion (assuming a gas coolant).

beam energy/amu	^{8}Li yield (Be)	^{8}Li yield (Cu)	^{8}Li yield (W)
30	30,204	23,153	34,051
40	49,539	46,028	75,416
50	86,333	75,777	132,151
60	144,571	112,004	206,666
	Be property	Cu property	W property
Melting point	1278 °C	1085 °C	3422 °C
Thermal conductivity	210 W/m·K	390 W/m·K	174 W/m·K

Table 6: A comparison of solid targets. Top: the ^{8}Li yield for 10^7 protons on target for different target materials and incident proton energies (considered in Sec. 4.2). Bottom: relevant material properties.

The ^{8}Li (or equivalently $\bar{\nu}_e$) event rate is shown for the various materials in Table 6. Despite its slightly lower ^{8}Li production rate, ease of handling the radioactive target underground has led us to consider beryllium as the most attractive choice among the materials studied. The p+W interaction will produce, in descending order of activation, ^{179}Ta, ^{173}Lu , ^{174}Lu, ^{157}Tb and ^{101}Rh [51]. These are significant radiation hazards; ^{157}Tb has a 100 year lifetime, while the others are between 1 and

5 years. Other problematic isotopes that are among the top 20 contributors of activation from W are ^{22}Na, ^{55}Fe, ^{60}Co, and ^{85}Kr [51]. These can be compared against the isotopes listed in Fig. 6, which are those that are produced in beryllium for 10^7 protons on target. The longest lived isotope produced is ^{11}C, with a 30 minute lifetime, and which is produced in very small quantities. As a result of the added complexity of radiation handling for tungsten, we expect that beryllium will be the more cost effective alternative. We note, however, that tungsten provides an alternative if power issues prove to be unsurmountable for a beryllium target. This issue will be studied in the future.

A radical alternative is a liquid mercury target. The primary argument for liquid mercury targets is dissipation of heat. However, these targets, such as the mercury one produced for the SNS, are very complex and expensive, and require a large hot-cell infrastructure for routine maintenance. The EURISOL-DS study gives cost accounting for various MW-level targets [52]. The associated cost of the liquid target components in the overall assembly total to $>$ \$30M, not including labor. Also, the target itself along with the associated components requires a large volume compared to the volume of beryllium needed for IsoDAR. This means a much larger radius of ^{7}Li would be required. For these reasons, a liquid target is impractical for IsoDAR.

4.3.2 Alternative Sleeve Materials

Initially, a borated polyethelene target sleeve was considered for the production of $\bar{\nu}_e$ via the neutron-capture-induced creation and subsequent decay of beta-emitting ^{12}B. As the neutron inelastic cross-section on ^{10}B is orders of magnitude higher than the neutron capture cross-section on ^{11}B, only ^{11}B was included in the sleeve material. This resulted in 403,628 ^{12}B isotopes produced for 10^7 incident protons. However, even a small contamination of 0.1% ^{10}B reduces ^{12}B production by a factor of $\sim$500. Recalling that stable boron is composed of 20% ^{10}B and 80% ^{11}B (and isotopic separation at the $>$99.9% level is not trivial), this material selection was not considered further. We also note that ^{10}B would need to be purchased whereas isotopically pure ^{7}Li is available in a substantial inventory for federal nuclear programs, and could possibly be "borrowed" much like the depleted uranium for the D0 experiment.

Several variations on the choice of lithium were studied. First, natural lithium was considered. As the neutron inelastic cross-section for ^{6}Li is much higher than the neutron capture cross-section on ^{7}Li, only 99 ^{8}Li isotopes per 10^7 protons on target are actually produced inside the sleeve with this material. This can be compared to the rates for 99.99% pure ^{7}Li shown in Fig. 6. We note that the four nines in "99.99%" can be considered a realistic goal for the sleeve. Fig. 9 shows the dependence of ^{8}Li yield on ^{7}Li isotopic purity. A LiO_2 target sleeve was also considered, but again the rates were not competitive with pure solid lithium.

5 Alternative Driver Designs

In this section, we investigate alternative options of accelerators that can be "drivers" in the IsoDAR system. The machines that could possibly produce sufficient current at high enough energy are cyclotrons, LINACS, FFAGs (Fixed Field Alternating Gradient), and RPSs (Rapid Cycling Synchrotron). Tandem van de Graaffs cannot reach the necessary current and are not considered.

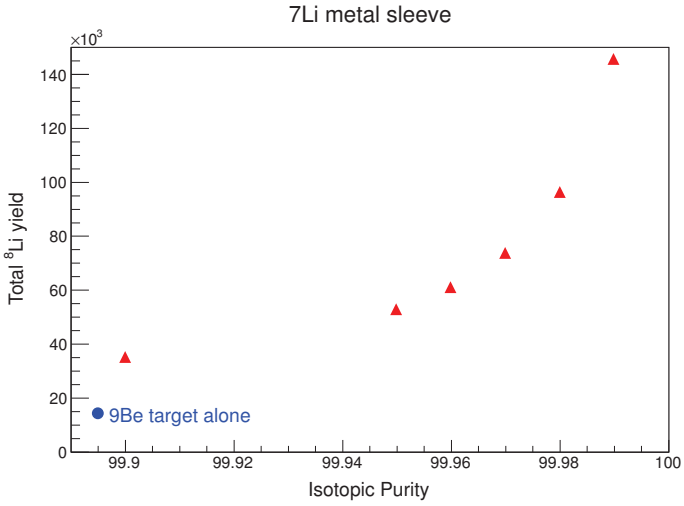

Figure 9: ^{8}Li yield for various ^{7}Li isotopic purities inside the target sleeve in the baseline IsoDAR design.

5.1 RFQ with Separated Sector Cyclotrons Running at 60 to 70 MeV

One of the limits for achieving high power in cyclotrons is the amount of beam that can be captured at low energies for acceleration. Conventional axial injection with a spiral inflector is subject to current limits from space-charge blowup, and emittance dilution because of phase-space coupling as the beam bends from the vertical direction to the horizontal cyclotron plane. These current limits have been thoroughly explored with proton and H^- beams injected into high-current cyclotrons used for isotope production; the typical limits (for $Q/A = 1$) for beams injected at 30 kV are around 2 mA. Using perveance (Eq. 1) to describe this, the higher the value of K, the more sensitive a beam is to space-charge effects. Taking this value of K for protons (and 2 mA current) and scaling this for H_2^+ (with Q/A = 0.5), we see that an electrical current of 5 mA (10 mA of protons) will have the same K value if the injection energy is raised to 35 keV/amu (terminal potential increased to 70 kV). This is the heart of the argument that H_2^+ beams will have substantially higher currents. An experiment is under construction at Best Cyclotron Systems in Vancouver [53] to verify this scaling (i.e. proof of the feasibility of high intensity H_2^+ injection using a spiral inflector). At the same time, we will further refine our numerical models for precise central region designs and parameter prediction for the IsoDAR cyclotron.

The simplest alternative approach is reducing current and increasing the injection energy. Eq. 1 shows that if the injection energy is increased from 35 to 800 keV/amu, K drops to only 1% of its original value, and injection space-charge issues become insignificant. This voltage would be too high to use a spiral inflector, but injection at higher energies is certainly feasible into a separated-sector cyclotron. The PSI Injector [54] is a good example: 12 mA of protons at 800 keV are injected into a separated sector cyclotron and ~ 3 mA are accelerated up to 72 MeV. The controlled losses (collimation) are at the first turns which do not produce high activation. Limits at PSI are determined by beam loss at the highest energies in the ring cyclotron and not by the performance of the injector cyclotron.

While PSI uses a Cockcroft-Walton platform to produce the energy of 800 keV, less expensive alternatives are possible today using RFQ accelerators. Such compact LINACs can be built now with parameters quite suitable for injection into a cyclotron, namely CW operation (100% duty

factor), with very low energy spread, and with an RF frequency that matches the optimum value for the cyclotron itself. In fact, the Indiana Cyclotron is injected by such an RFQ, manufactured by AccSys Inc [55], an accelerator company located in Pleasanton, CA.

A preliminary look at the IsoDAR configuration using an RFQ injecting a 4-sector ring cyclotron indicates costs could increase by 40% or more from the baseline. With this said, the RFQ-injection alternative does provide a path forward in case the BEST Cyclotron Systems tests show an issue with the spiral inflector injection.

5.2 LINACs With Low Energy (30 MeV) and High Current (40 mA)

Proton LINACs can provide the correct combination of beam energy and current for reaching the necessary $\bar{\nu}_e$ flux. These machines are long chains of accelerating RF cavities, where each cavity increases the beam energy by as much as a few MeV. To increase electrical efficiency, modern high current LINACs are superconducting and therefore markedly decrease wall current losses, and thereby increase the electrical efficiency.

As compared to cyclotrons, LINACs can provide much higher current with the same level of losses. This is because strong transverse-focusing can be applied using quadrupole magnets placed throughout the line. Also, relatively strong longitudinal focusing is produced by the high frequency of the RF cavities. This can be compared to the cyclotron, where both transverse and longitudinal focusing are weak and therefore space charge is challenging to control at injection. The result is that the limit of current in the LINAC will be largely set by the output of the ion source. In this discussion, we assume that 40 mA can be accelerated. Using Table 8, this sets our LINAC energy at 30 MeV.

The size of a LINAC is driven by the fact that the beam passes through the line only once. This necessarily requires a long machine, with many cavities, and high power needs are inevitable for both the RF and the cryogenic systems (for superconducting machines). The length is a function of beam energy and the accelerating gradient. The superconducting cavities offer higher gradients, reducing the length by a factor of three. Using the ESS as our example, the high current LINAC length is 27 m for 50 MeV in energy [56].

A study by the IAEA [57] considered a d-beam at $\sim$25 MeV, accelerated by a LINAC, on ^{7}Li as a neutron generator. The quoted cost for such a machine is ">\$50M for 100 kW of power on target". The most relevant high power, low energy ion accelerator being designed is the International Fusion Materials Irradiation Facility (IFMIF). IFMIF draws heavily from the experience at the LEDA at Los Alamos. The cost-scaling from the IFMIF design work is >\$100 M. As a reference point for the cost of RF-power and cryogenics, one can consider the costs for the Jefferson Lab CEBAF Upgrade, which was \$5M for the complex of 13 kW RF-amplifiers, which would be needed for IsoDAR [58]. This leads to the same conclusion, namely that this solution will cost far more than \$50M and is therefore not cost-effective.

5.3 FFAGs

We have also considered a FFAG accelerator design. Such a machine would resemble a sector cyclotron, the difference being that the magnetic field varies radially as well as azimuthally. In some sectors the field increases with radius; in other sectors it decreases. This alternating gradient produces strong focussing, so that the bunches in such machines are better contained than they are in a cyclotron, and losses are lower. If the scaling requirement –that the optics of the beam is independent of energy– is relaxed, then there is considerable freedom in the choice of magnetic field configuration. If this field configuration is chosen carefully the design can also be isochronous,

so the machine can operate continuously at a fixed RF frequency. The relaxation of scaling means that the particle bunch will pass through tune resonances during its acceleration. However, if the acceleration is fast then this need not be fatal, as has been shown by the success of the EMMA prototype [59, 60]. This combination of focussing and CW operation, the best features of the synchrotron and the cyclotron, make the FFAG a very appealing choice for IsoDAR.

However, experience with FFAG machines is still limited. EMMA is an electron machine, and does not experience the problems of varying velocity, or space charge, that is expected with IsoDAR. The proton machines constructed at KURRI [61] have operated successfully in the energy range we require, but have only achieved currents in the nA-range. An FFAG for IsoDAR would involve a new design and a considerable R&D program. We will continue to investigate the possibility of an FFAG - it may be that other applications and industries will be interested and drive these developments. However, the FFAG concept is still insufficiently proven for us to adopt it in preference over an established cyclotron design.

5.4 Rapid Cycling Synchrotrons

Fig. 10 shows the context in which cyclotrons and rapid cycling synchrotrons are employed. The machines are mapped in energy-current-beam power parameter space. The upper left corner (in red) is the domain of fixed B-field cyclotrons. In the classic Lawrence design the uppermost energy achievable is between 10 to 20 MeV depending on the RF-voltage. At higher energies the beam loses synchronism with the RF. Synchronism can be restored by varying the frequency of the RF (green area). The energy reach up to 1 GeV comes at the expense of much reduced beam current as only a single bunch can be in the machine at any one time. The upper energy is limited by the declining extraction efficiency as the beam orbits get closer together. At 1 GeV, the extraction efficiency of the Dubna machine has fallen to 30%. Much higher energies can be achieved in proton synchrotrons.

The highest energy extracted beam (800 GeV) was possible with the Tevatron. The beam current in these machines is limited by the Laslett incoherent tune shift at injection that is in turn set by the beam emittance and injection energy. The Tevatron had the capability of delivering an average current of up to 500 μA in pulses at 1 Hz. Lower energy, rapid cycling synchrotrons have been proposed and built with pulsed beams at rates approaching 100 Hz. The maximum current, again limited by the incoherent tune shift, is $\sim$300 μA.

Achieving very high power, especially at low proton energy, requires a machine capable of accelerating 1 to 10 mA. This regime is the province of cyclotrons with a radially and azimuthally varying B-field that provides stronger edge focusing of the beam and assures synchronism with a fixed RF-source over the entire acceleration cycle. Such machines with both resistive and superconducting magnet coils are mainstays of the research and medical industries. Extraction efficiencies, even at hundreds of MeV, exceed 99.9%. Machine reliability and availability is also very high ($\sim$95%). The proposed DAEδALUS and IsoDAR accelerators are of this variety and build on decades of experience with this proven accelerator technology.

6 Radically Different Designs

The previous discussion centered on maintaining the basic IsoDAR design while replacing individual elements. In this section, we consider radically different designs.

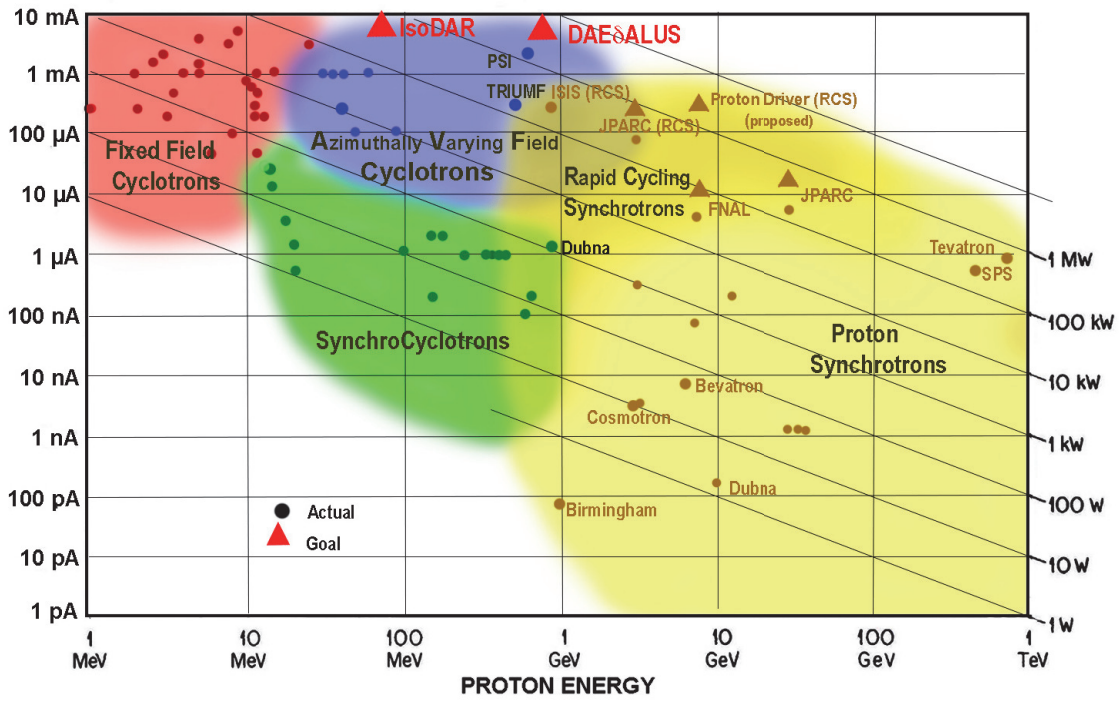

Figure 10: Current versus proton energy for various existing machines. Various types of cyclotrons are shown; FF is the Fixed Field or Classical Cyclotron; FM is the Frequency Modulation (Synchro-) Cyclotron; and AVF is the Azimuthal Varying Field Cyclotron. One can see that IsoDAR is far from the space populated by Rapid Cycling Synchrotons. This is an updated version of Fig. 1 from Ref [62].

6.1 Why Not Use the β-beam Production Design?

Designers of β-beam technology have studied the production of ^{8}Li using a 25 MeV beam [63]. Perhaps IsoDAR could use the reaction $^7\mathrm{Li}(d,p)^8\mathrm{Li}$ to produce the necessary flux at 25 MeV? In this section, we explore this possibility and ultimately conclude that it is not feasible.

The β beam is produced by impinging a ^{7}Li beam on a gas deuterium target to produce ^{8}Li, for subsequent acceleration. This type of reaction, where the beam is more massive than the target, is referred to as "reverse kinematics." The 25 MeV energy is just above Coulomb barrier in the center of mass system for this asymmetric target-beam species. Beta beams obviously need as much motion *in* the center of mass frame as possible, for boosting acceleration and kinematic focusing to form a beam; however, this is irrelevant and in fact not desirable for the case of IsoDAR. A gas target is used so that the relatively fast outgoing ^{8}Li isotope can be extracted for acceleration. The ^{7}Li is stored in a recirculating ring in order to increase the rate [64].

There are two issues which cause us to reject this base design. Even with the recirculating design, the maximum production will be about 3×10^{21} ions per year [63], which is 10 times lower than the baseline IsoDAR flux. Therefore, it is a high-risk assumption that solutions could be found to increase rates by an order of magnitude. Further, the system requires a two accelerator chain, first to reach 25 MeV, and then to recirculate the beam. This will increase cost, add complexity, and enlarge the necessary footprint of the design and leads us to the conclusion that adapting this recirculating-beam-gas-target design for IsoDAR would be much more expensive than the baseline

cyclotron system proposed.

On this basis, we reject the use of the β-beam design. However, we can now investigate designs "inspired" by the planned β-beam production.

6.1.1 ^{7}Li Beam on a Liquid Deuterium Target

A small LINAC could be used to accelerate ^{7}Li up to $\sim$25 MeV to impinge on a liquid deuterium target. However, we conclude that this is not a cost-effective option as LINACs are quite expensive (discussed in Sec. 5.2) and because maintaining a cryogenic liquid target in a system that absorbs nearly 1 MW of beam power is challenging.

Why not use a tandem accelerator since this would be less expensive than an RF LINAC? A tandem is a high impedance device which therefore delivers low beam currents continuously. A high current tandem might deliver 10 μA. The advantage of the tandem is extreme voltage stability (0.5%) that can be important for low energy nuclear physics, when one wants to sit on a resonance. However, such an accelerator does not fulfill the requirements of IsoDAR.

6.1.2 Deuteron Beam on a ^{7}Li Target

Classic measurements of the reaction d+^{7}Li$\rightarrow$ p+^{8}Li have been done with few MeV beams on solid lithium targets [65]. A low energy beam is appropriate for exploiting resonances of hundreds of millibarns in the deuteron energy region of 3-4 MeV. However, low energy deuterons range out very quickly, penetrating < 0.5 mm into target. Energy loss moves the deuteron through the resonance quickly, so that $< 0.1\%$ of the beam particles interact to produce ^{8}Li. In the designs we have explored, the rates of ^{8}Li production are two orders of magnitude lower than the baseline IsoDAR design.

6.2 Use of Existing or Planned Accelerators and a New Detector

The last alternative to consider is whether it is more cost-effective to build a new detector at an existing accelerator facility or build a new accelerator at an existing large scintillator-based detector as is proposed for IsoDAR.

A cyclotron and a 1 kton "KamLAND-like" detector, such as the one proposed for OscSNS [66], are approximately the same cost. This can be seen by comparing the cost estimates in Ref. [66] and Ref. [36]. Thus, the issue is not in the cost of the equipment itself, it is in the cost of the implementation.

Oil-based detectors at the surface require small-duty factor beams because of backgrounds produced by spallation from cosmic-ray muons and from decays of stopping muons. The IsoDAR source cannot make use of a small duty-factor beam because the half-life of ^{8}Li is 841 ms. Therefore, the flux will be continuous, regardless of beam structure, unless the beam bunch spacing is significantly more than 1 s. There are no existing facilities that offer 600 kW of beam power at $\sim$ 60 MeV with pulsed spacing of $\gg 1$ s. With the 6% duty factor for LSND, achieving 600 kW at 60 MeV would require 160 mA of current on target.

It is for this reason that scintillator detectors used with continuous beams are built underground. Recent examples are the modern reactor experiments, which have very similar rates of IBD interactions in their far-detector halls as IsoDAR. The Double Chooz far hall is at 300 mwe depth [67], the RENO far hall is at 450 mwe [68] and the Daya Bay EH3 far hall is at 860 mwe [69]. These choices set the scale for the range of acceptable depth for a detector accomplishing IsoDAR-like physics.

A new detector that meets IsoDAR's physics goals would need to be installed hundreds of feet underground. There is no existing facility where this civil construction would be cheap. One can consider the cost estimates for the near hall of LBNE, which was proposed to be 185 ft below grade, to see that this hall would be a very expensive project. Along with the experimental hall, a new beamline would be required to bring the beam to the detector as well. For these reasons, we do not consider deploying a new detector at an existing accelerator as cost-effective.

7 Discussion and Conclusions

We now compare the IsoDAR design to the most often suggested alternative proposals: the RFQ/Separated Sector Cyclotron design; a LINAC design; a modified β-beam design using a low energy deuteron beam on a ^{7}Li target; and a new detector, matching KamLAND specifications, built under 300 m.w.e shielding at an existing accelerator laboratory.

As shown in Fig. 11, we roughly classify the designs considered as "good" (green), "moderate" (yellow), or "bad" (red) for each criterion. The meaning of the grade for each criterion is described below:

- *Cost:* Good: $\sim$ \$30M, Moderate: $\sim$ \$50M, Bad: $\sim$ \$100M or higher. The cost estimates can be considered very rough. Plausibility of the IsoDAR estimate can be cross checked against the D.O.E. cost study of a 70 MeV, 1 MW cyclotron [36]. In the case of a new experiment, the cost includes a new beamline and an underground site, as well as the KamLAND-like detector.

- *$\bar{\nu}_e$ Rate in 5 years:* Good: $\gtrsim 1 \times 10^{23}$; Moderate: $\sim 5 \times 10^{22}$; Bad: $< 1 \times 10^{22}$.

- *Backgrounds:* For IsoDAR and the first four comparisons, Good: $< 1\%$ ν_e; Moderate: $< 5\%$ ν_e; Bad: $> 5\%$ ν_e with endpoint > 3 MeV. In the case of a new detector, the background at 300 mwe will overwhelm the singles signal. However, the background should be adequate for the IBD-based measurements, and is therefore marked as moderate.

- *Low technical risk:* Good: Very little R&D required, uses proven technology; Moderate: Modest R&D required, uses cutting-edge technology; Bad: Significant R&D needed, uses unproven technology. IsoDAR makes use of the new VIS source, and is therefore marked as moderate.

- *Compactness of both accelerator and source:* Good: Expect very little underground excavation; Moderate: requires new rooms of conventional size; Bad: requires major construction. For the new beamline, new detector alternative, we assume the laboratory will have sufficient space on site.

- *Simplicity of underground construction and operation:* Good: Excellent modularity; Moderate: must plan around some large pieces; Bad: many large pieces that do not fit through tunnels.

- *Reliability:* Good: 95% uptime typical, so unlikely to be an issue; Moderate: 90% uptime typical, so could be the limiting factor; Bad: <90% uptime, so the limiting factor. All of the designs are expected to be highly reliable except for the modified β-beam design which is likely to have significant technical difficulties.

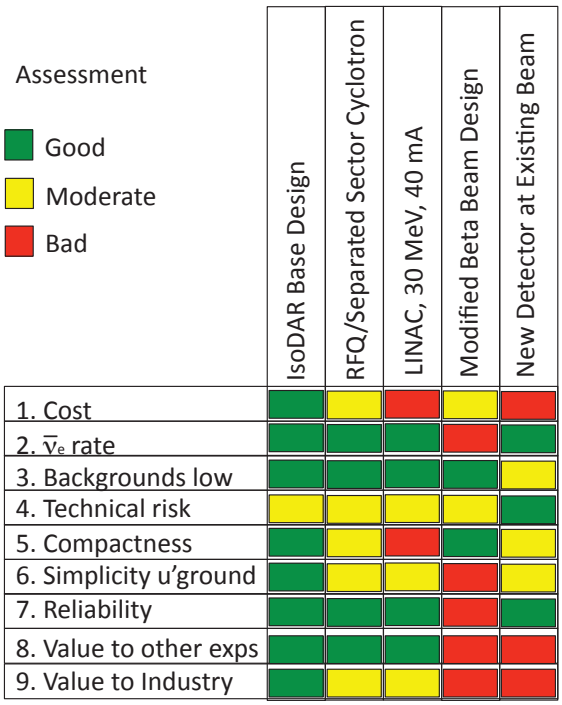

Figure 11: Comparison of IsoDAR to alternative designs. See text for explanation.

- *Value to future physics programs:* Good: multiple examples of applications in physics; Moderate: one other example; Bad: no examples. In the case of IsoDAR, these include application of the technology to DAEδALUS and to rare isotope production facilities such as Legnaro, Holifield, and the 70 MeV cyclotron in Nantes.

- *Value of this development to industry:* Good: multiple examples of interested industries; Moderate: one other example; Bad: no examples. In the case of IsoDAR, the IBA and BEST Cyclotron Systems companies have both demonstrated interest in the design.

Based on this study, we conclude that the IsoDAR base design is the best technology choice for the planned physics application.

References

[1] A. Bungau *et al.*, Phys. Rev. Lett. 109, 141802 (2012).

[2] S. Abe *et al.* [KamLAND Collaboration], Phys. Rev. Lett. 100, 221803 (2008).

[3] http://physics.aps.org/synopsis-for/10.1103/PhysRevLett.109.141802

[4] J.M. Conrad, J.M. Link and M.H. Shaevitz, Phys. Rev. D. 71, 073013 (2005).

[5] J. Barranco, O.G. Miranda, C.A. Moura and J.W.F. Valle, Phys. Rev. D 73, 113001 (2006).

[6] A. de Gouvea and J. Jenkins, Phys. Rev. D 74, 033004 (2006).

[7] A.E. Nelson and J. Walsh, Phys. Rev. D 77, 033001 (2008).

[8] N.E. Davison, M.J. Canty, D.A. Dohan, and A. McDonald, Phys. Rev. C 10, 50 (1974).

[9] Yu S. Lutostansky and V.I. Lyashuk, The Bulletin of the Russian Academy of Sciences 75, 468 (2011).

[10] N.G. Basov and V.B. Rozanov, JETP Lett. 42, 431 (1986).

[11] M. Abs *et al.*, arXiv:1207.4895 [physics.acc-ph].

[12] J. Alonso *et al.*, [DAEδALUS Collaboration], arXiv:1006.0260 [physics.ins-det].

[13] J.M. Conrad and M.H. Shaevitz, Phys. Rev. Lett. 104, 141802 (2010).

[14] A. Gando *et al.* [KamLAND Collaboration], Phys. Rev. D **83**, 052002 (2011).

[15] C. Bemporad, G. Gratta, and P. Vogel, Rev. Mod. Phys. 74, 297 (2002).

[16] R. Miracoli *et al.*, Rev. Sci. Instrum. 83, 02A305 (2012).

[17] T. Mitsumoto, K. Fujita, T. Ogasawara, H. Tsutsui, S. Yajima, A. Maruhashi, Y. Sakurai, and H. Tanaka, Proceedings of CYCLOTRONS 2010, Lanzhou, China, FRM2CCO04 (2010).

[18] Beam loss when crossing resonances is discussed in many textbooks. See, for example, D.A. Edwards and M.J. Syphers, *Introduction to High Energy Accelerators*, John Wiley & Sons, 1993.

[19] J.J. Yang, A. Adelmann, W. Barletta, L. Calabretta, and J.M. Conrad, arXiv:1209.5864 [physics.acc-ph].

[20] J.J. Yang, A. Adelmann, M. Humbel, M. Seidel, and T.J. Zhang, Phys. Rev. ST Accel. Beams 13, 064201 (2010); http://amas.web.psi.ch/docs/opal/user-guide-html/

[21] Y.J. Bi, A. Adelmann, R. Dölling, M. Humbel, W. Joho, M. Seidel, and T.J. Zhang, Phys. Rev. ST Accel. Beams 14, 054402 (2011).

[22] http://www.iba-radiopharmasolutions.com/products-cyclo/cyclone-30

[23] http://www.advancedcyclotron.com/cyclotron-solutions/tr30

[24] T. Kuo, Private Communication.

[25] S. Ituru, Private Communication.

[26] A. Adelmann, Private Communication.

[27] V. Sabaiduc, *et al.,* "High Current Operation of the TR30 Cyclotron," Conference on Cyclotrons and Their Applications, 2007.

[28] W.T. Chu, S.B. Curtis, J. Llacer, T.R. Renner, and R.W. Sorensen, "Wobbler facility for biomedical experiments at the Bevalac" PAC 85, pp 3321-3323 (1985).

[29] B.W. Blackburn, "Characterization of a high-current tandem accelerator and the associated development of a water-cooled beryllium target for the production of intense neutron beams", Thesis (M.S.)–Massachusetts Institute of Technology, Dept. of Nuclear Engineering, 1997. http://hdl.handle.net/1721.1/44487

[30] S. Agostinelli *et al.*, Nucl. Instr. & Meth. A 506, 250 (2003).

[31] Evaluated Nuclear Data File ENDF/B-VII, www.nndc.bnl.gov/endf

[32] The GEANT4 medical applications page is https://twiki.cern.ch/twiki/bin/view/Geant4/Geant4MedicalPhysics. An in-depth explanation of the GEANT4 medical application settings, which are also appropriate for IsoDAR, appears in C. Jarlskog and H. Paganetti, IEEE Trans. on Nuc. Sci, 55, 1018 (2008); An expanded discussion of the GEANT4 neutron settings appears in S. Garny, G. Leuthold, V. Mares, H.G. Paretzke, W. Ruhm, IEEE Trans. on Nuc. Sci, 56 2392 (2009). Examples of relevant benchmark data for neutron production by protons on beryllium are: S.W. Johnsen, Med. Phys. 4, 255 (1977) and H.I. Amols, J.F. Dicello, M. Awschalom, L. Coulson S.W. Johnsen, and R.B. Theus, Med. Phys. 4, 486 (1977).

[33] http://www.iba-cyclotron-solutions.com/products-cyclo/cyclone-70

[34] http://www.bestcyclotron.com/product_70p.html

[35] J.R. Alonso, arXiv:1209.4925 [nucl-ex].

[36] "Cost/Benefit Comparison for 45 MeV and 70 MeV Cyclotrons," Conducted by Jupiter Technical, Security and Management Solutions for the U.S. Department of Energy, Office of Nuclear Science, Energy and Technology, www.isotopes.gov/outreach/reports/Cyclotron.pdf (2005).

[37] F. Poirier *et al.*, "C70 Arronax in its Hands On Phase," http://accelconf.web.cern.ch/accelconf/IPAC2012/papers/moppd024.pdf; L. Medeiros Romao *et al.*, "IBA C70 Cyclotron Development," Conference on Cyclotrons and their Applications, 2007. http://accelconf.web.cern.ch/accelconf/c07/PAPERS/54.PDF

[38] http://www.phy.ornl.gov/hribf/initiatives/cyclotron/cyclotron-upgrade.pdf

[39] http://web.infn.it/spes/

[40] L. Calabretta, D. Rifuggiato, M. Maggiore, and V. Shchepounov, "A superconducting ring cyclotron to deliver high intensity proton beams," Proceedings of EPAC 2000, Vienna, Austria.

[41] http://itheo.org/thorium-energy-conference-2011

[42] See, for example, M. Martone, M. Angelone, and M. Pillon, "The 14 MeV Frascati Neutron Generator", Journal of Nuclear Materials 212B, 1661 (1994).

[43] S.-I. Meigo, *et al*, "Beam Commissioning of Spallation Neutron and Muon Source in J-PARC", Proceedings of PAC09, Vancouver, BC, Canada, TU6PFP066 (2009).

[44] Yves Jongen, Thierry Delvigne, Pascal Cohilis, "Multi-milliampere compact cyclotrons used as neutron sources", Society of Photographic Instrumentation Engineers, Vol 2339, 225-235 (2011).

[45] Phil Ferguson, Private communication.

[46] R. Alba, M. Barbagallo, P. Boccaccio, A. Celentano, N. Colonna, G. Cosentino, A. Del Zoppo and A. Di Pietro *et al.*, arXiv:1208.1713 [nucl-ex].

[47] R. Baartman, F. Bach, Y. Bylinsky, J. Cessford, G. Dutto, D. Gray, A. Hurst, K. Jayamanna, M. Mouat, Y. Rao, R. Rawnsley, L. Root, R. Ruegg, and V. Verzilov, "Reliable production of multiple high intensity beams with the 500 MeV TRIUMF Cyclotron", Cyclotrons 2010, Lanzhou, 280-282.

[48] M. Seidel Ch. Baumgarten, M. Bopp, J. Grillenberger, Y. Lee, D. Kiselev, A. Mezger, H. Muller, M. Schneider, and A. Strinning, "Towards the 2 MW cyclotron and latest developments at PSI", Cyclotrons 2010, Lanzhou, 275-279.

[49] R.W. Garnett, L.J. Rybarcyk. D.E. Rees, T. Tajima, and E. Pitcher, "High-power options for LANSCE", PAC-11, New York, 2107-2109.

[50] Yan Zhang for SNS accelerator team: "Experience and lessons with the SNS Superconducting LINAC", IPAC 2010, Kyoto, 26-30.

[51] N. Shetty, R. Nabbi, and B. Thomauske, "Interaction of High Energy Proton Beam in a Spallation Target," http://www.inbk.rwth-aachen.de/publikationen/Shetty_Nabbi_High_Energy_Proton_Beam_2011.pdf

[52] K. Samec, *et al.*, "EURISOL-DS Multi-MW Target Cost Analysis for a Proposed Development Phase", EURISOL-DS/TASK2/TN-02-25-2009-046, EN-Note-2009-009 STI (2009).

[53] http://www.bestcyclotron.com/

[54] L. Stingelin, M Bopp, and H. Fitze, "Development of the new 50 MHz Resonators for the PSI Injector II cyclotron", Cyclotrons and their applications, 18th conference, Giardini Naxos, Italy, Oct 1-5 2007, 467-469.

[55] http://www.accsys.com/

[56] E. Baussan, M. Dracos, T. Ekelof, E. Fernandez Martinez, H. Ohman, and N. Vassilopoulos, "Proposal to use the a high intensity neutrino beam from the ESS proton LINAC for measurement of neutrino CP violation and mass hierarchy," Submitted 31 July 2012 to the Open Symposium on the European Strategy for Particle Physics in Krakow, September 10-12, 2012.

[57] IAEA Publication, "Development opportunities for small and medium scale accelerator driven neutron sources: Report of a technical meeting held in Vienna, 1821 May 2004", IAEA-TECDOC-1439.

[58] R. Rimmer, "Accelerator costs", International Workshop on Accelerator-Driven Sub-Critical Systems & Th Utilization (2010).

[59] S. Machida *et al.,* Nature Physics Vol. 8 243 (2012).

[60] J.M. Garland, H. Owen, D. Kelliher, S. Machida, and B.D. Muratori, "An Experimental Investigation of Slow Integer Tune Crossing in the EMMA Non-Scaling FFAG". In Proc. International Particle Accelerator Conference, 2012.

[61] M. Tanigaki *et al.,* Proc. European Particle Accelerator conference 2006, p. 2367-2369 (2006).

[62] F.T. Howard, Nuclear Instruments and Methods, 18, 125 (1962).

[63] M. Lindroos and M. Mezzetto, Ann. Rev. Nucl. Part. Sci. 60, 299 (2010).

[64] C. Rubbia, A. Ferrari, Y. Kadi and V. Vlachoudis, Nucl. Instrum. Meth. A 568, 475 (2006).

[65] B.W. Fillipone, A.J. Elwyn, W. Ray, Jr., and D.D. Koetke, Phys. Rev. C 25, 2174 (1982).

[66] I. Stancu *et al.* [OscSNS Collaboration], "The OscSNS White Paper" (2008).

[67] Y. Abe *et al.* [Double Chooz Collaboration], Phys. Rev. Lett. 108, 131801 (2012).

[68] J.K. Ahn *et al.* [RENO Collaboration], Phys. Rev. Lett. 108, 191802 (2012).

[69] F.P. An *et al.* [Daya Bay Collaboration], Phys. Rev. Lett. 108, 171803 (2012).